

VMC

Venus Monitoring Camera on Venus Express

Anomalous features in the VMC images

VMC-MPAE-TN-SS010-001

Issue 3/1

04.08.2008

Prepared by: D. Titov

Document Change Record

Iss./Rev.	Date	Chapter	Description
1/	26.04.06		Description of the anomalies in the VMC images
2	03.05.2006		Preliminary analysis of the causes
3/0	30.05.2006		Fig 2-12 and text
			Fig 2-13 and text
3/1	04.08.2008		Appendix A. Artifacts in the VMC images (from PhD Thesis by R. Moissl)

Table of contents

1	Scope of the Note	5
2	Dark stripe	5
2.1	Appearance and properties	5
2.2	Analysis of the UV dark stripe anomaly	7
2.2.1	Width of the stripe	7
2.2.2	Orientation	7
2.2.3	UV sensitivity degradation versus exposure to the sun.....	11
2.2.4	Properties of the CCD detector.....	15
3	Dark spots and filaments	17
3.1	NIR-1 channel.....	17
3.2	NIR-2 channel.....	17
3.3	UV channel	18
3.4	Visible channel	18
3.5	In orbit stray light images.....	19
3.6	First pericentre images.....	20
3.7	Analysis of the spots and filaments structures.....	21
3.7.1	Properties and behaviour	21
3.7.2	Temperature limits of the CCD	22
3.7.3	VMC thermal model	22
3.7.4	Thermo-vacuum tests at MPS.....	23
3.7.5	Spacecraft TB/TV tests.....	23
3.7.6	Sun illumination test.....	23
3.7.7	In-flight temperature monitoring	25
4	Conclusions	26
5	Appendix A. Artifacts in VMC images (from R. Moissl's PhD thesis).....	28
5.1	A.1 Dark UV strip	28
5.2	A.2 Filament-spot patterns	30

1 Scope of the Note

The first VMC images of Venus taken in Capture orbit, during in orbit commissioning and first pericentre pass as well as the in-orbit stray light images showed a number of anomalous features that were not present during the last stray light test in February 2006. Two types of features were observed:

1. Dark stripe crossing the image in the UV channel only;
2. Dark spots and filaments randomly scattered over the field of view of all four channels;

This Note describes the appearance and properties of the mentioned features and proposes analysis of the factors that possibly led to the degradation of VMC performance.

2 Dark stripe

2.1 Appearance and properties

The horizontal dark stripe appears in all UV images. Example is shown in figure 2.1.



Figure 2.1 UV image of Venus v0001_0076.uv2 taken in Capture orbit.

The dark stripe crosses the image horizontally (almost perpendicular to the CCD columns) and has width of ~18 pixels at half-minimum (figure 2.2).

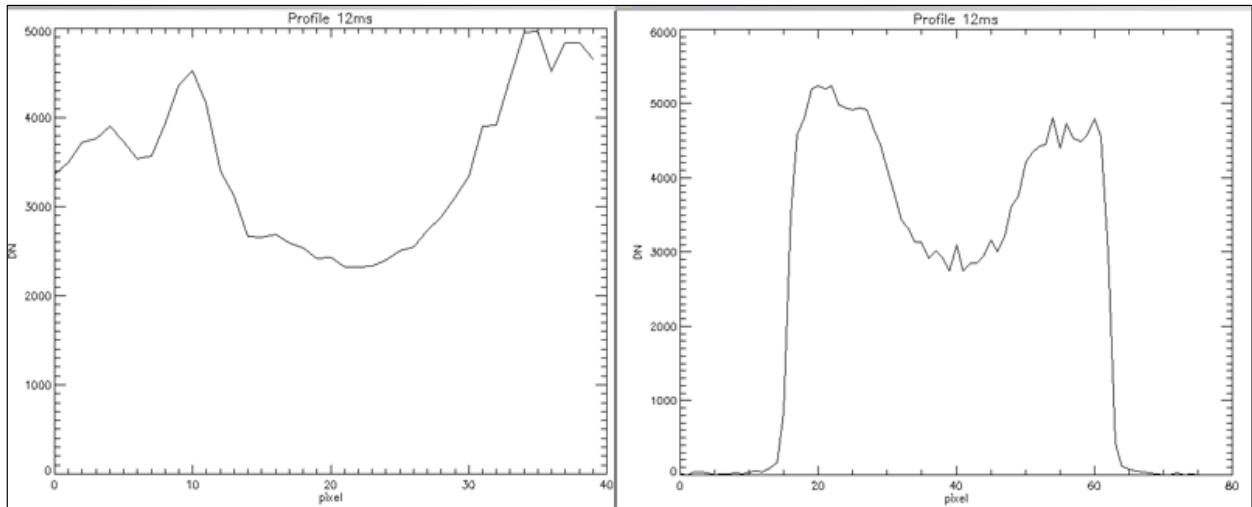


Figure 2.2 Brightness profiles across the CCD perpendicular to the dark stripe (right).

Although inside the dark stripe the features on the Venus disc are visible and recognizable its centre is characterized by about a factor of 2 lower sensitivity as compared to the rest of the image. Figure 2.3 shows the appearance of the dark stripe when the entire field of view was illuminated during the stray light tests on April 24, 2006.

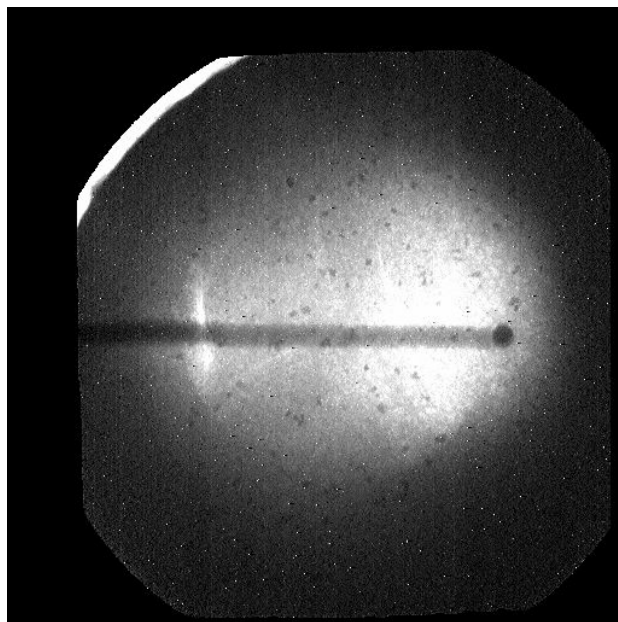


Figure 2.3 UV image v0002_0010.uv2 taken during in-orbit stray light characterization on April 24, 2006.

Figure 2.4 shows the UV image taken during the pericentre pass when Venus fully occupied the VMC field of view.

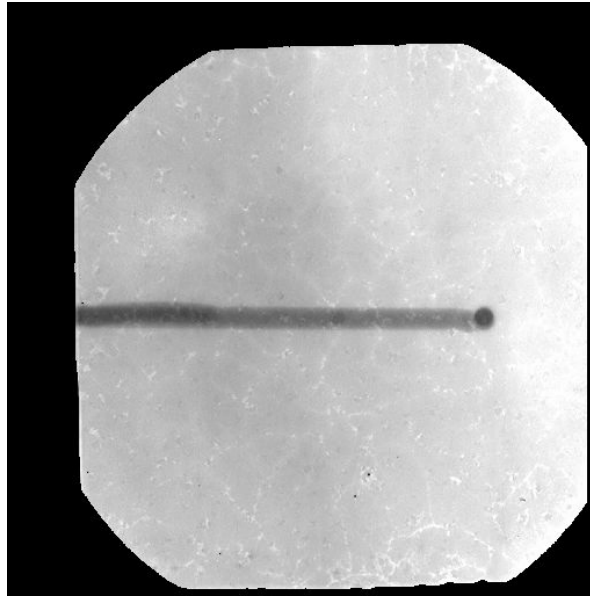


Figure 2.4 UV image v0004_0033.uv2 taken during the first pericentre pass.

2.2 Analysis of the UV dark stripe anomaly

Current working hypothesis is that the dark stripe represents the track of the sun image that slowly traveled across the CCD during the Venus approach in March-April 2006 and resulted in degradation of the detector sensitivity in illuminated pixels due to exposure of intensive UV light. The size of the stripe and its orientation support this explanation.

2.2.1 Width of the stripe

Angular dimensions of the sun as seen from Venus is ~ 13 mrad that corresponds to ~ 17 pixels of the CCD. This is almost exactly the width of the dip in the dark stripe brightness profile (figures 2.2, 2.3).

2.2.2 Orientation

The dark stripe is oriented perpendicular to the columns of the CCD which are parallel to the Y axis of the spacecraft. Thus the dark stripe is oriented in the XZ plane in which the sun was kept during the approach phase (so-called power optimized spacecraft orientation). Figure 2.4 shows the evolution of the angle between Earth and Sun as seen from the spacecraft (magenta curve). When the angle was close to 90 degrees (end of March-beginning of April) the sun was close to the +Z axis of the spacecraft shining directly in the VMC field-of-view.

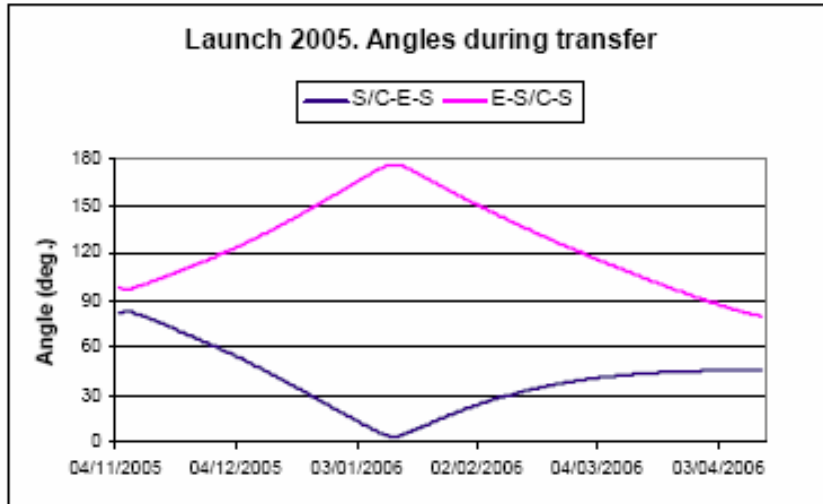


Figure 5-4: Communication angles during interplanetary trajectory. Launch 2005.

Figure 2.5 Earth-spacecraft-Sun angle during the cruise phase.

VMC: Front View on CCD Photosensitive Area, Co-ordinate System and Pixel Numbering

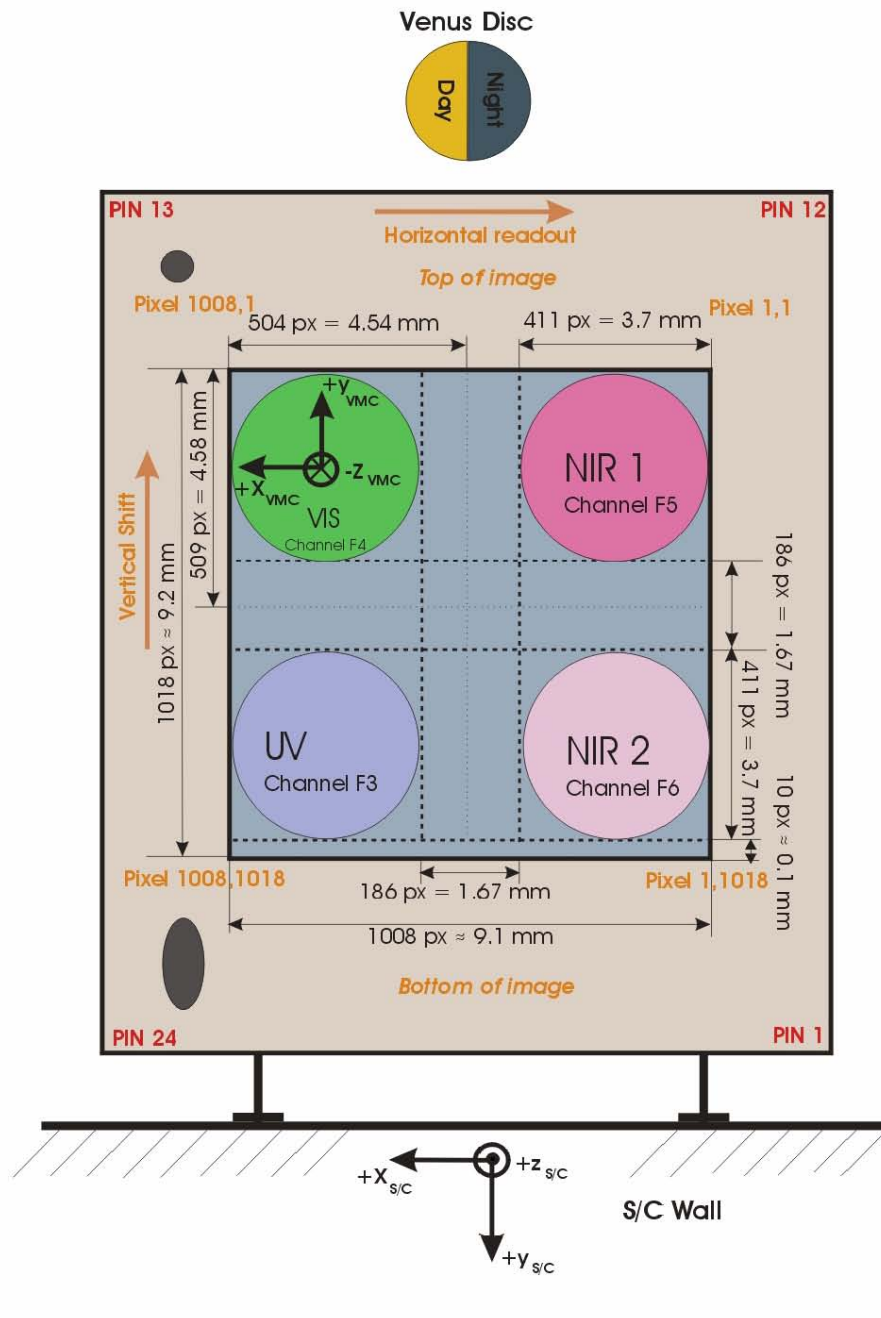


Figure 2.6 CCD orientation wrt spacecraft coordinates. CCD columns are vertical in this figure

Analysis of the VMC Spice kernels allowed us to reconstruct the apparent motion of the Sun image on the UV quadrant of the CCD and to determine total solar illumination load for each pixel (figures 2.8, 2.9)

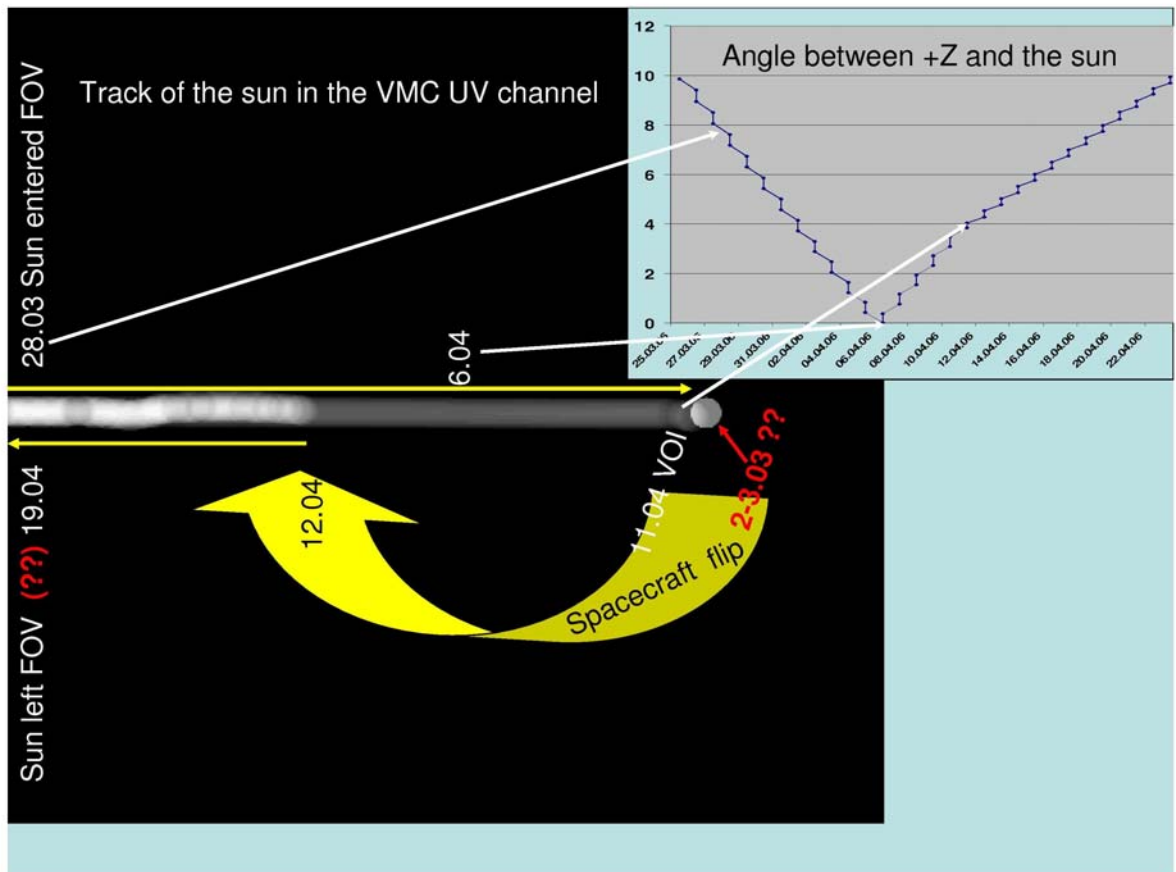


Figure 2.7 Track of the Sun image on one quadrant of the CCD reconstructed from the Spice kernels. Brightness of the stripe marks total illumination load. Venus disc is shown schematically.

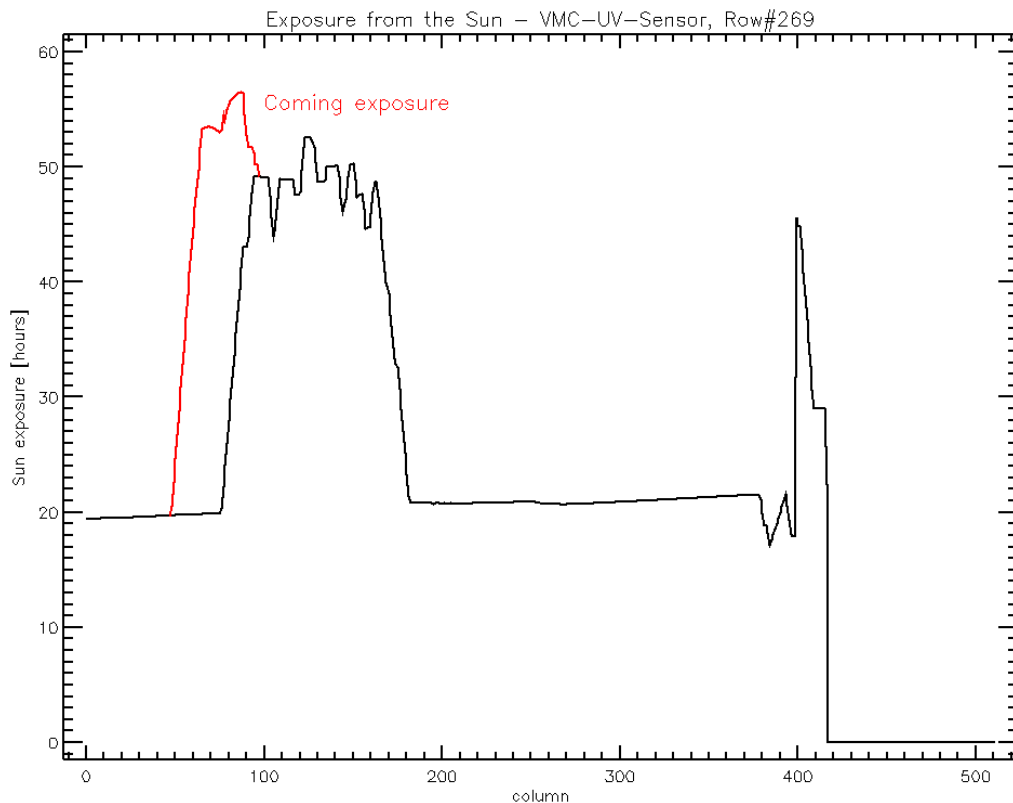


Figure 2.8 Exposure of the UV quadrant to the Sun illumination between March 1 and April 19, 2006 reconstructed from the Spice kernels. Venus disc is shown schematically.

2.2.3 UV sensitivity degradation versus exposure to the sun

Figure 2-8 above shows the degradation of the sensitivity of the pixels as a function of exposure to the sun. Although the data is very scattered two quasi-linear regions can be seen. 0-20 hours seems to have somewhat steeper slope than the region 20-60 hours. This could imply that we may reach a non-zero asymptote at certain point.

It is clear from the plot that the effect is accumulative (see section 2.2.4)

Further, it is also clear that degradation is already significant after exposure to the sun for several hours. For this reason we need to avoid exposure to the sun of this order.

It not however clear if there is a threshold for the effect. All of the pixels with sun exposure greater than 60 seconds come from the strip of the sun track as seen in Figure 2-7. There are however other pixels that have been exposed to the sun during several reorientations of the S/C (slews and possibly VMC stray light test). The slews tracks are shown in Figure 2-10. The corresponding pixel vs sun exposure plot is shown in Figure 2-11. From this Figure we see that the maximum of the DN values decreases with sun exposure but the minimum does not. This

seems to be contradictory in the first instance. However looking carefully from which part of the slews tracks these pixels come from we find that the pixels with sun exposure greater than 30 sec come from a somewhat darker part of the image (left lower corner) and hence have a lower maximum. We can therefore conclude that the CCD sensitivity degradation is within the noise for these pixels. We can not however say anything about potential accumulation of the degradation effect.

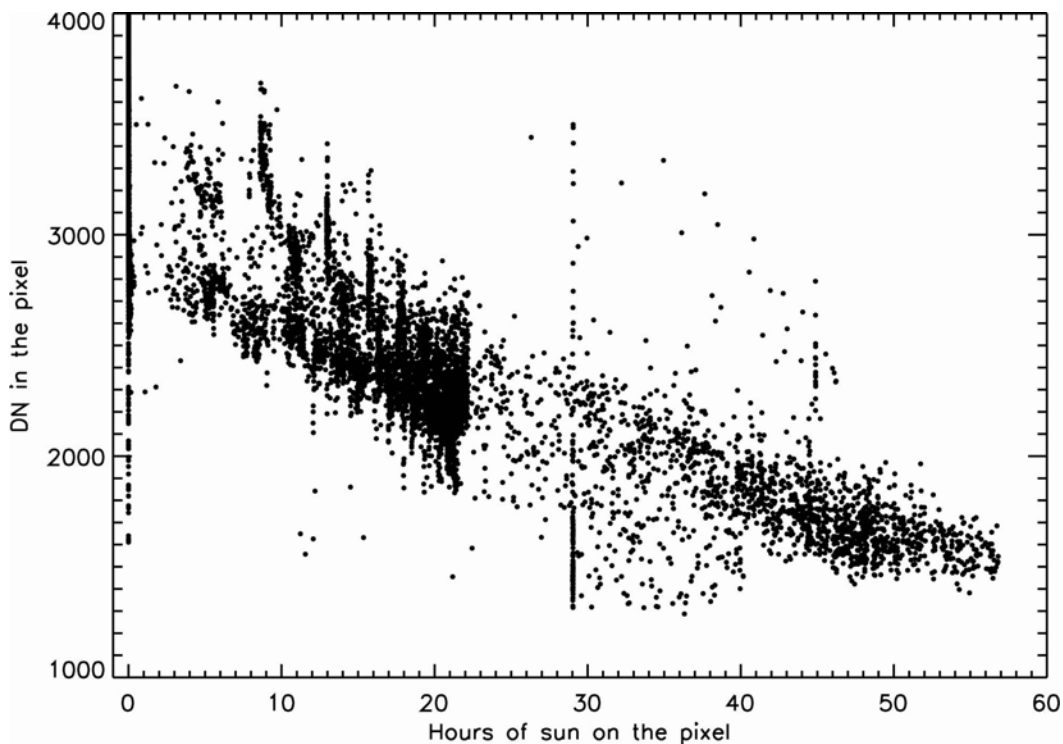


Figure 2.9 DN in the pixel vs hours the pixel was exposed to the sun.

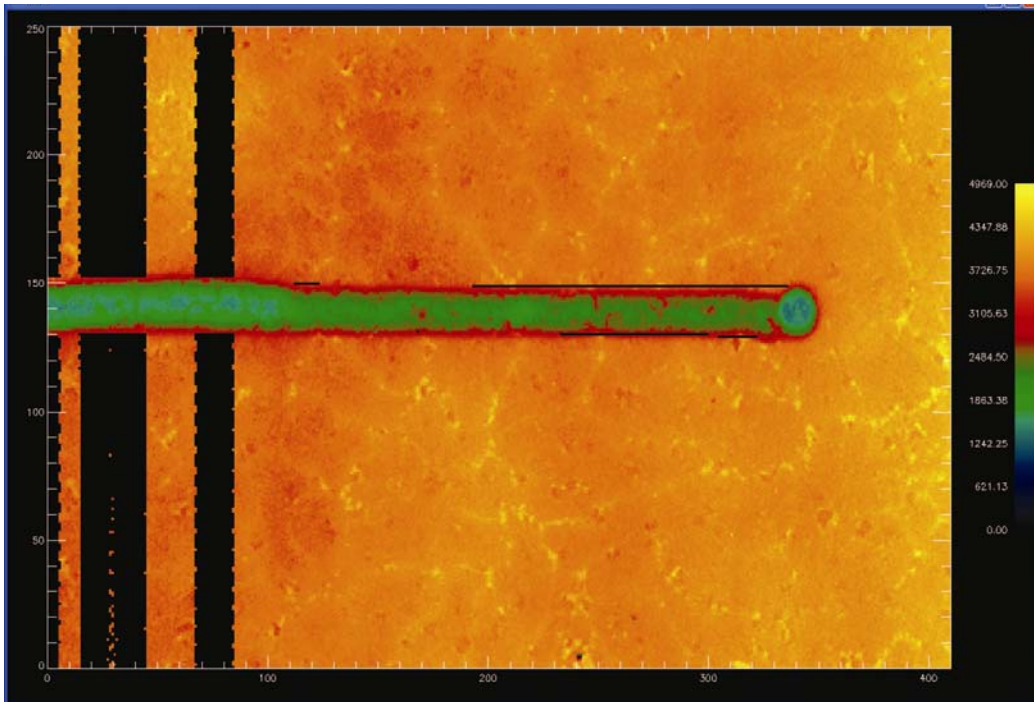


Figure 2.10 See text for details

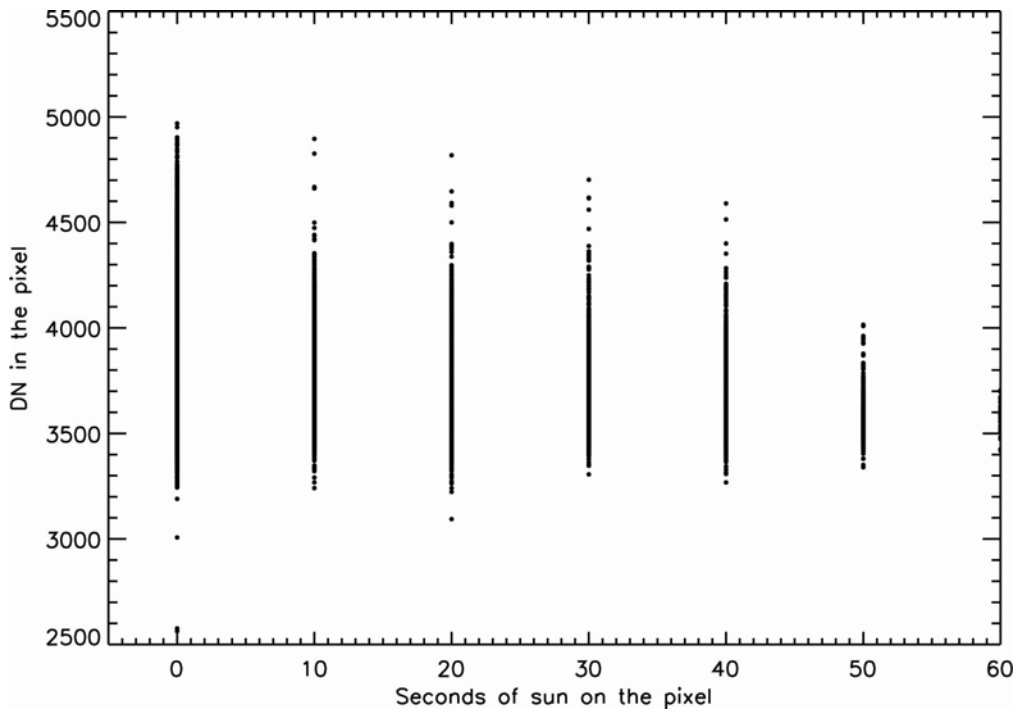


Figure 2.11 Pixels effected by slews with sun exposure of less than 60 seconds.

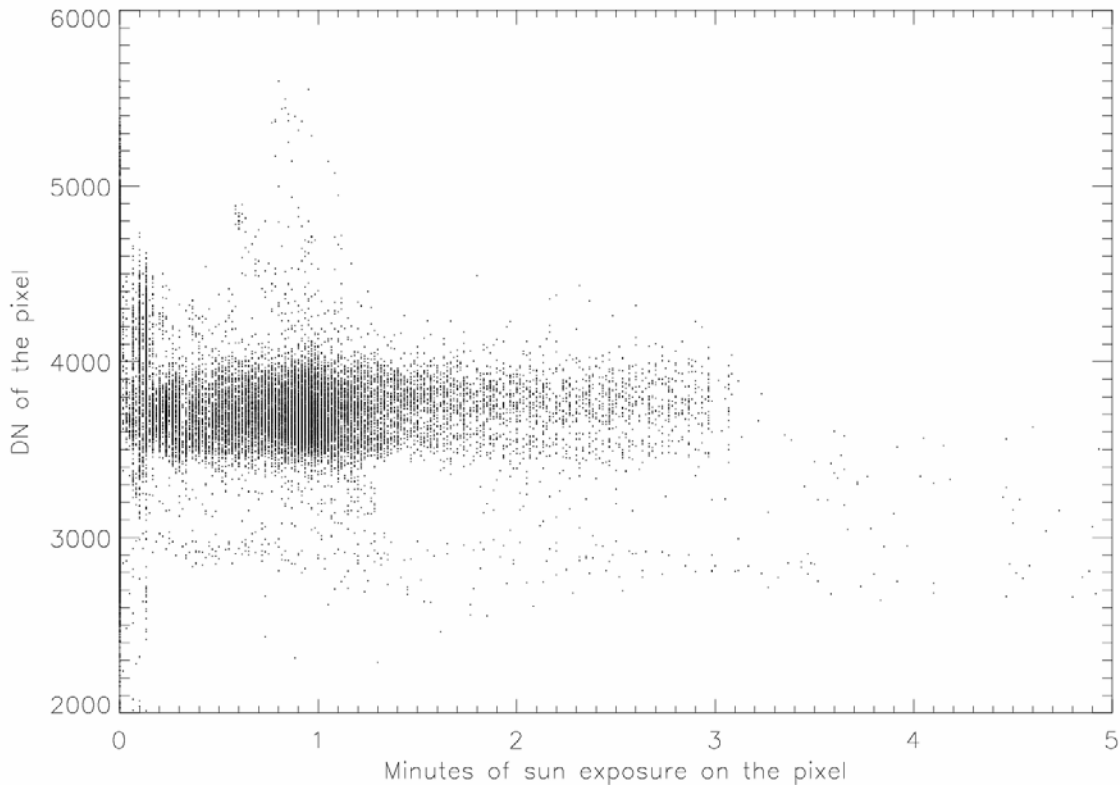


Figure 2.12 Similar to Figure 2-11 but going out to five minutes and with sampling of every second.

In Figure 2-12 we show all pixels exposed to the sun for five minutes or less. The sampling in time is now every second. The pixels exposed to the sun for more than 1 minute are those in the neighborhood of the main stripe (Figure 2-10). It can be concluded that a few minutes exposure to the sun does not degrade the CCD sensitivity. It can not be excluded however that effect may accumulate with repeated short exposures to the sun.

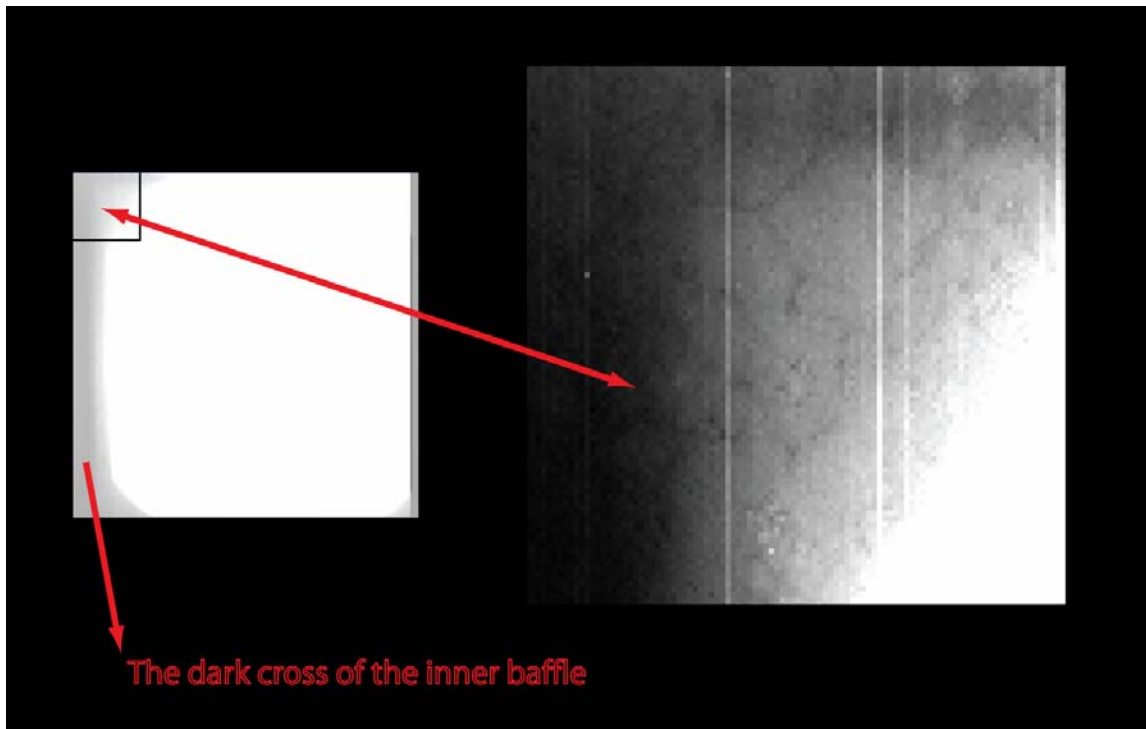


Figure 2.13 UV channel. A very overexposed image. Stray light illuminated area underneath the cross. The pattern is visible.

Left side of Figure 2-13 shows a very saturated UV VMC image. There was so much stray light that even the dark area underneath the inner baffle was partially illuminated. The honeycomb pattern is visible there. Since this area is not illuminated directly it would seem to exclude that the pattern is on any of the optical surfaces and must be on CCD. We have not however been able to show this for the other channels. This may be simply due to the fact that the signal is very weak.

2.2.4 Properties of the CCD detector

VMC uses KODAK KAI-1010M monochrome detector. Discussion with KODAK led to the conclusion that the detector spectral responsivity in blue range can degrade under long term exposure to the sun light due to discoloring of the microlenses that cover the chip. After 14 days exposure to 50 Klux sunshine the CCD quantum efficiency decreased from 33% to 22% at 400 nm (the lowest wavelength considered by KODAK). Extrapolation of this trend to the wavelength of VMC UV channel (365 nm) results in decrease of sensitivity from ~25% to ~10%. The following three factors should be applied to re-scale the 14 days exposure in the KODAK experiments to the actual exposure in the VMC UV channel.

1). Distance factor. 50Klux illumination that KODAK used in its aging tests corresponds to 39% of solar constant outside the Earth atmosphere (127 klux) or 20% of the solar flux in Venus orbit, i.e. the distance factor is 0.2.

2). Optical factor. The ratio of the size of the sun image on the CCD ($r \sim 10$ pixels = $90 \mu\text{m} = 0.09$ mm, $s = 0.025 \text{ mm}^2$) to that of the aperture of the VMC UV channel ($r = 2$ mm, $S = 12.56 \text{ mm}^2$) is $g = s/S = 0.002$. Taking into account the UV channel transmittance of $\sim 30\%$ the VMC optics the optical scaling factor will be 0.0067

3). Spectral factor. We assume that KODAK used solar spectrum in its aging tests. No investigating of spectral dependence of this process was performed. VMC UV filter bandpass is ~ 30 nm. Assuming that the CCD microlenses are affected by the UV and visible light (300-600 nm) we get the spectral scaling factor of 10.

So the total scaling factor is 0.013. Hence, 14 days (336 hours) of 50 klux illumination in the KODAK aging tests are approximately equivalent to ~ 4 hours of sun illumination of one CCD pixel.

3 Dark spots and filaments

The figures below show the appearance of dark spots in four quadrants of the CCD. For each channel two images are shown: the left one corresponds to the first slot of observations in Capture orbit. The right image is one of the last taken in Capture orbit. Note that the figures 3.1 – 3.8 show only central part of the CCD about 100x100 pixels.

3.1 NIR-1 channel

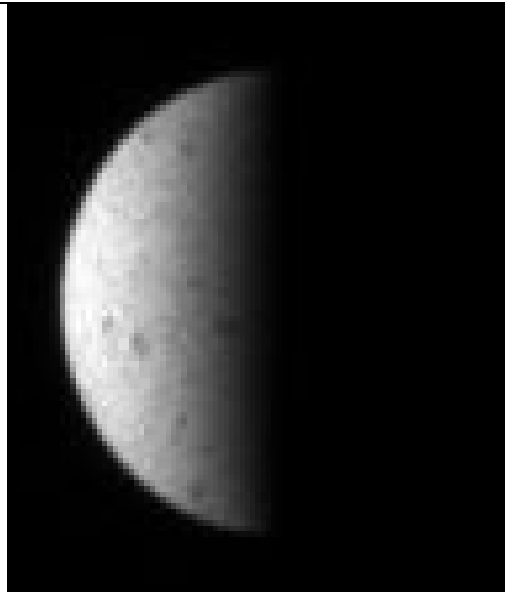


Figure 3.1 v0000_0006.n12



Figure 3.2 v0001_0006.n12

3.2 NIR-2 channel



Figure 3.3 v0000_0007.n22

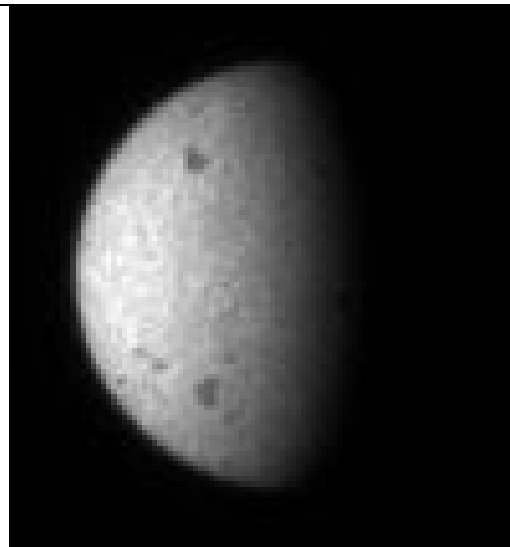


Figure 3.4 v0001_0007.n22

3.3 UV channel



Figure 3.5 v0000_0004.uv2



Figure 3.6 v0001_0004.uv2

3.4 Visible channel



Figure 3.7 v0000_0000.vi2

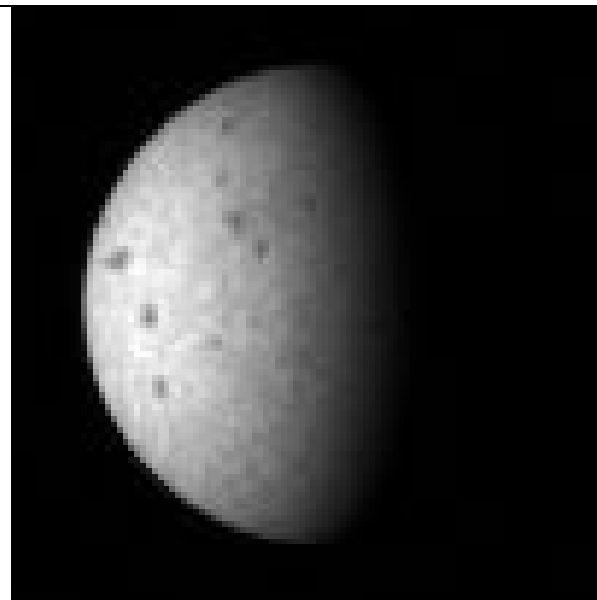


Figure 3.8 v0001_0000.vi2

3.5 In orbit stray light images

In-orbit stray light measurements gave the first opportunity to see the above mentioned features in the whole FOV. Figure 3.9 -3.12 show the dark spots randomly spread in all four channels.

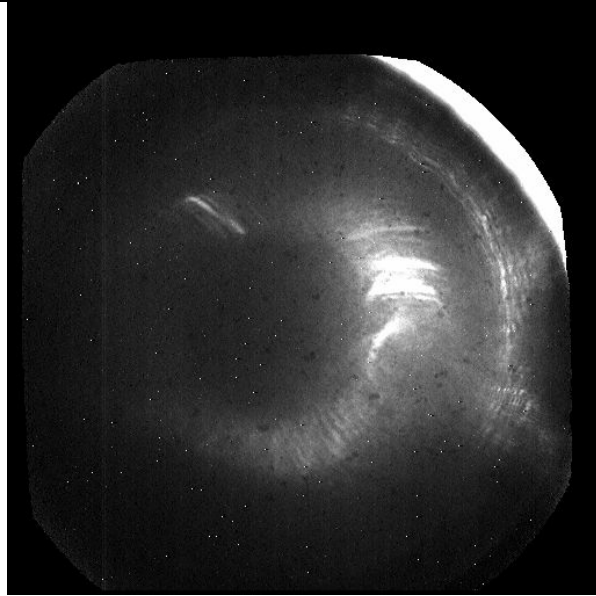


Figure 3.9 NIR2 image v0002_0010.n22

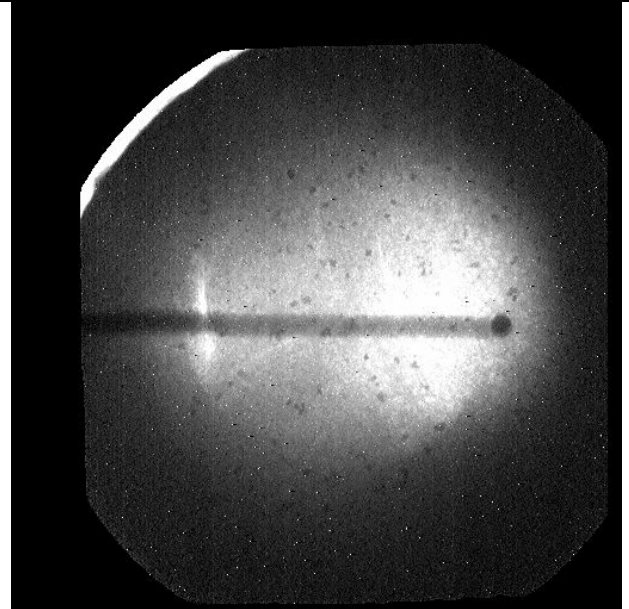


Figure 3.10 UV image v0002_0010.uv2

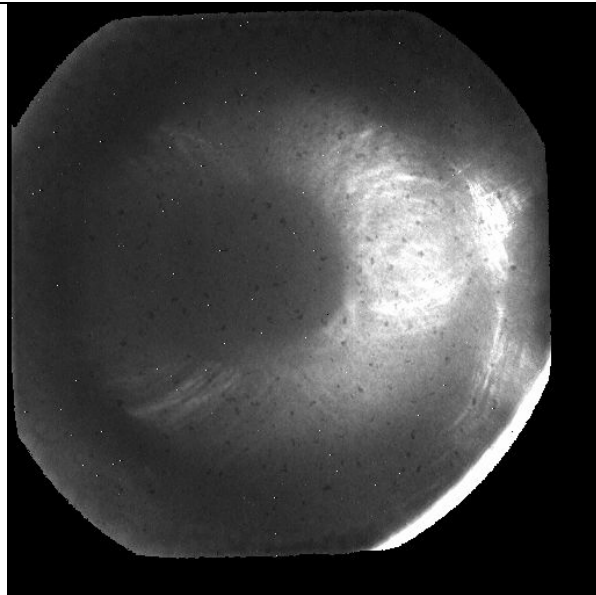


Figure 3.11 NIR1 image v0002_0010.n12

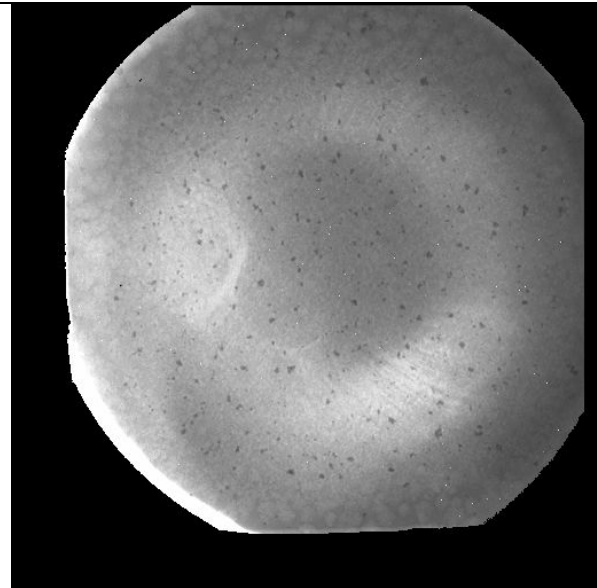


Figure 3.12 Vis image v0002_0010.vi2

Typical spot size is ≤ 5 . Sensitivity loss inside the spot area as compared to surroundings is between 30 and 70 %.

3.6 First pericentre images

The first pericentre images taken by VMC (Figures 3.13-3-17) gave a chance to see the changes in the flat field since Venus at close distance is relatively uniform object.

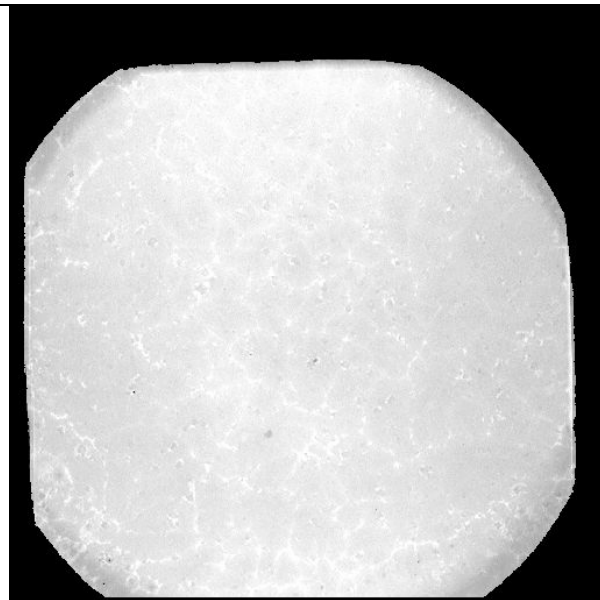


Figure 3.13 NIR2 image v0004_0002.n22

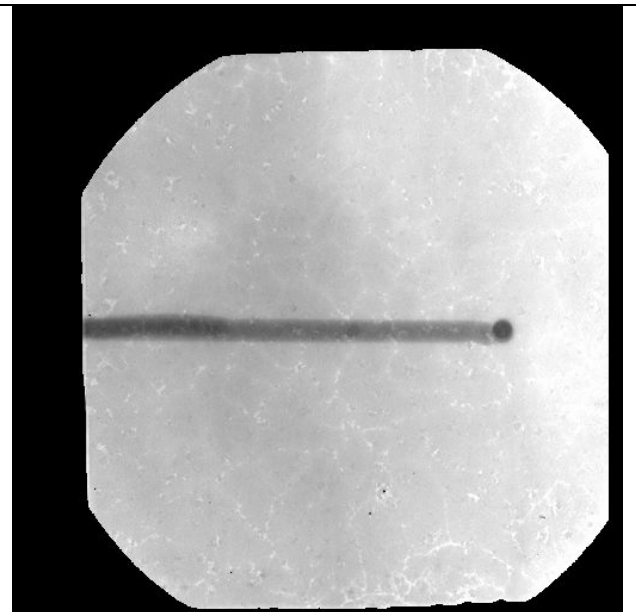


Figure 3.14 UV image v0004_0033.uv2

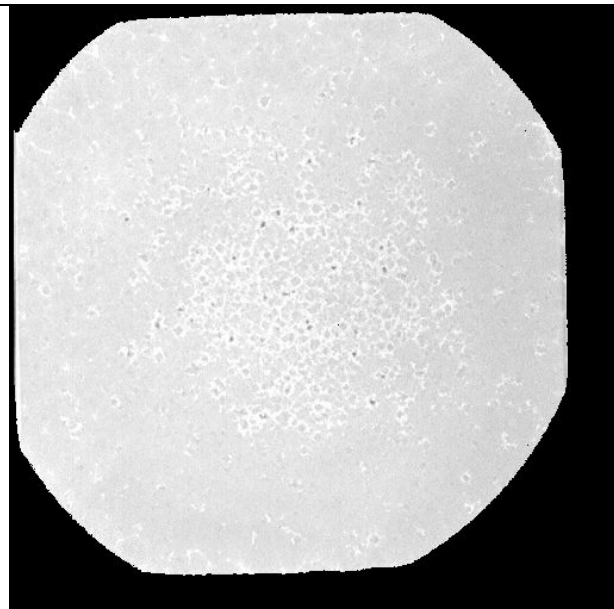


Figure 3.15 NIR1 image v0004_0000.n12



Figure 3.16 Vis image v0004_0003.vi1

3.7 Analysis of the spots and filaments structures

3.7.1 Properties and behaviour

The most prominent features seen in figures 3.13-3.17 are the sun track in the UV image, spots and filament structures. Spots and filaments are visible in all VMC channels, but the details of these structures vary from channel to channel. Positions of the spots observed in the first pericentre images (figs. 3.13-3.17) correlate with the dark spots observed in the Capture orbit (figs. 3.5-3.8) and stray light images (figs. 3.9-3.12).

We have looked at the evolution of spatial distribution during the time from launch to end of April 2006 (including orbit 8). They are not present in the stray light test in November. They are present starting with the stray light test in February 2006. We have identified some that have moved and some that have disappeared looking at the stray light test data taken in April. This would imply that they are loose particles on the surface of the CCD. On the other hand they are not or very poorly visible in the Venus images. Possible explanation is that they can only be seen when scene brightness is very low (as in stray light tests). Further analysis and future data are needed to understand exactly what they are.

In the first pericentre images the spots appear brighter. In the UV images the filaments cross the dark stripe that indicates that the processes that formed both were independent. Sharpness of the structures indicates that they are unlikely to be on the VMC optics but are rather on the CCD detector. Discussions with the optics manufacture (FISBA, Switzerland) confirmed this conclusion. See Appendix A for more details about the behaviour of the filament structures during the course of the mission.

There are three working hypothesis about the origin of the spots and filaments:

1. During the cruise phase the CCD temperature increased to the temperatures high enough for the CCD polymer coating and/or microlenses on the chip to melt.
2. In cruise the CCD and microlenses experienced strong thermal gradients that resulted in damaging of the polymer coating and/or microlenses.
3. Temperature increase in some parts of VMC due to sun illumination or operations resulted in evaporation of some material with its subsequent deposition on the CCD.

In order to verify these assumptions we analyze below the results of the laboratory thermal tests and in-flight temperature measurements as well as the manufacturer data about the temperature

limits of the CCD and its coating and information about the materials used in VMC manufacturing.

3.7.2 Temperature limits of the CCD

According to the KODAK data sheet for the KAI-1010M detector the ‘operations without damage’ range is -50C...+70C, and storage range is -55...+70C. The coating of the CCD surface and microlenses can withstand temperatures up to 150C.

3.7.3 VMC thermal model

The VMC thermal model was developed and included in the spacecraft model. The model and results of the test runs are described in the Chapter 5 of the VMC PID-B (VMC-MPAE-ID-SA020-001_1, issued 01.05.03). In the full orbit modeling (section 5.5.4.2) the “hot” case was modeled. It included the hottest conditions at TRP (+Y wall) during the pericentre pass and frontal illumination of the VMC front baffle and the optics during 11 hours of telecommunication phase (2-13 hours orbital time). Figure 3.17 shows the results of the thermal modeling of the hottest case.

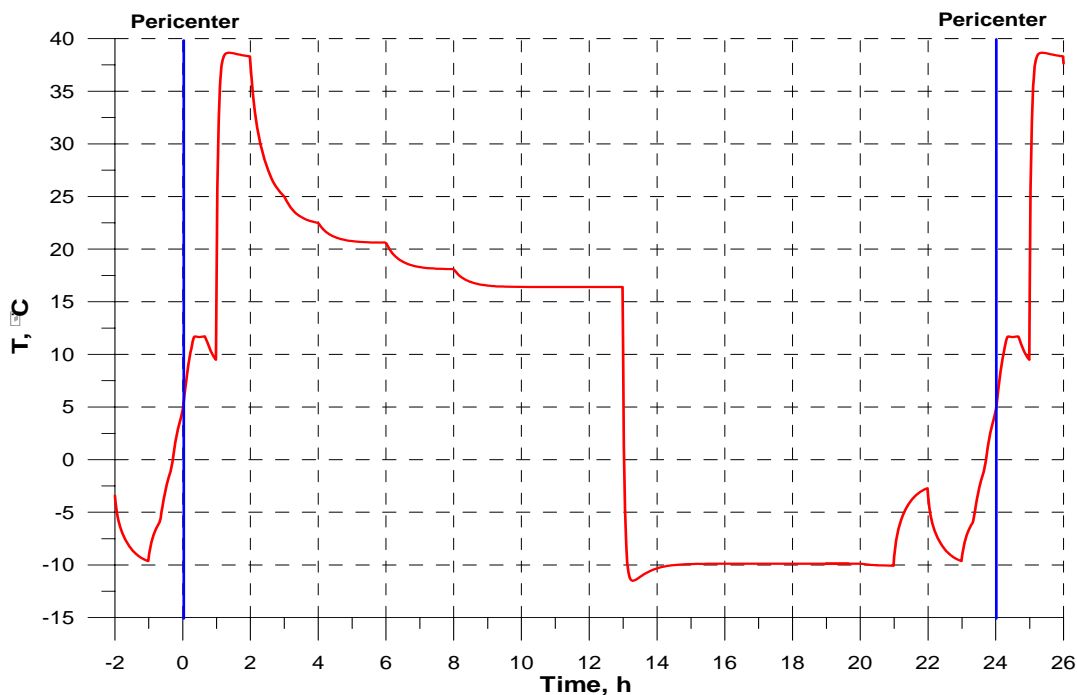


Figure 3.17. CCD temperature during the “hottest” case modeling.

The main conclusions derived from the thermal modeling are:

- Thermal regime of the CCD is defined by the temperature of the TRP on +Y wall and that of electronic boards;
- The increase of CCD temperature due to direct solar illumination is about few degrees.

We note however that later spacecraft TB/TV tests showed that the VMC thermal model underestimated the front baffle temperatures by ~20C. The reason for this discrepancy is still not clear and is being investigated.

3.7.4 Thermo-vacuum tests at MPS

The VMC instrument was tested according to the agreed verification programme that included thermo-vacuum tests with non-operational cycles between -50C and +65C, and operational tests for TRP temperatures from -40 C to +45C. The test reports VMC-MPAE-RP-SS010-002_1_a and VMC-MPAE-TN-SS010-001_2 are included in the VMC FS DRB data package. The instrument remained fully functional during and after the tests. No signs of CCD damages were recorded.

3.7.5 Spacecraft TB/TV tests

Correlation of the Astrium thermal model with the results of the spacecraft TB/TV tests led to the conclusion that the correlation on the VMC TRP is good but the thermal model of the front baffle underestimates by 22C the baffle temperatures during direct solar illumination. The work on clarifying the reason for this discrepancy is in progress. However, the front baffle is mounted on the VMC front plate and such temperature uncertainties cannot influence the temperature regime of the CCD which is enough to explain the observed degradation of the detector by thermal issues.

3.7.6 Sun illumination test

A specific test to prove that VMC can withstand direct solar illumination and does not require a shutter was conducted on the QFM model. Test report VMC-MPAE-RP-SF030-001_1 is also included in the VMC FS DRB data package. The test consisted of exposure of the VMC to frontal illumination of artificial “sun” with the flux equivalent to the one at Venus. The solar beam was ~10 degrees. The instrument was off. The temperatures were monitored on the CCD (via spacecraft thermistors), in several places on the back side of the front baffle, on the front

plate and on the TRP. The test lasted for 11 hours that was supposed to simulate the sun illumination during the Cebreros telecommunications. The quality of the flat field was controlled before and after the sun illumination test.

These tests were representative from the point of view of radiative heat load on the front baffle, front edge of the optical unit, lenses, and mean energy input on the CCD. Since the solar beam was much broader than the sun (0.75 degrees) the test was not representative from the point of view of a thermal load on illuminated pixels. However the estimates showed that due to small diameter of the optics and narrow bandpass the energy that reached CCD pixels is very small and can cause temperature difference of no more than 1K between the image of the sun and non-illuminated pixels.

The results of the tests were summarized as follows:

1. Maximum temperature of 69C was measured on the front baffle;
2. CCD temperature did not exceed 20 C;
3. No changes of the flat field that exceed the noise level were identified in the Visible and both NIR channels.
4. The UV channel after the test showed three places with darkening (figure 3.18). Theses spots were attributed to the plasmocere particles deposited on one of the lenses.
5. The VMC survived sun illumination test and was fully operational after the tests.

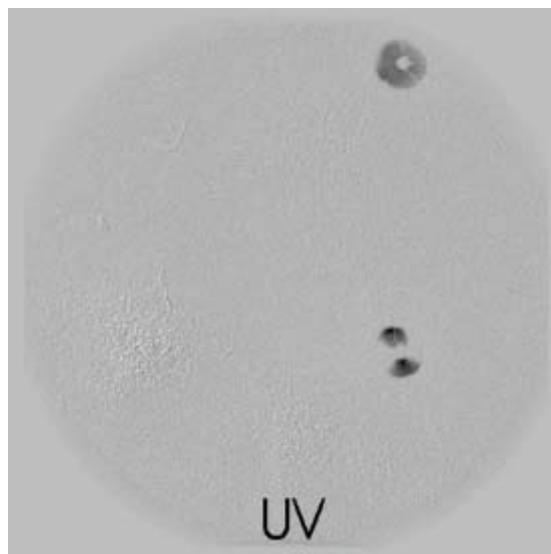


Figure 3.178. Difference between the flat field images after and before the sun illumination test.

3.7.7 In-flight temperature monitoring

The CCD temperature was permanently monitored by the spacecraft thermistors located on the CCD housing and DPU. Figures 3.19 and 3.20 show VMC temperature changes during cruise phase and first orbit operations. The CCD temperature never exceeded +40C that is well with the detector operational limit.

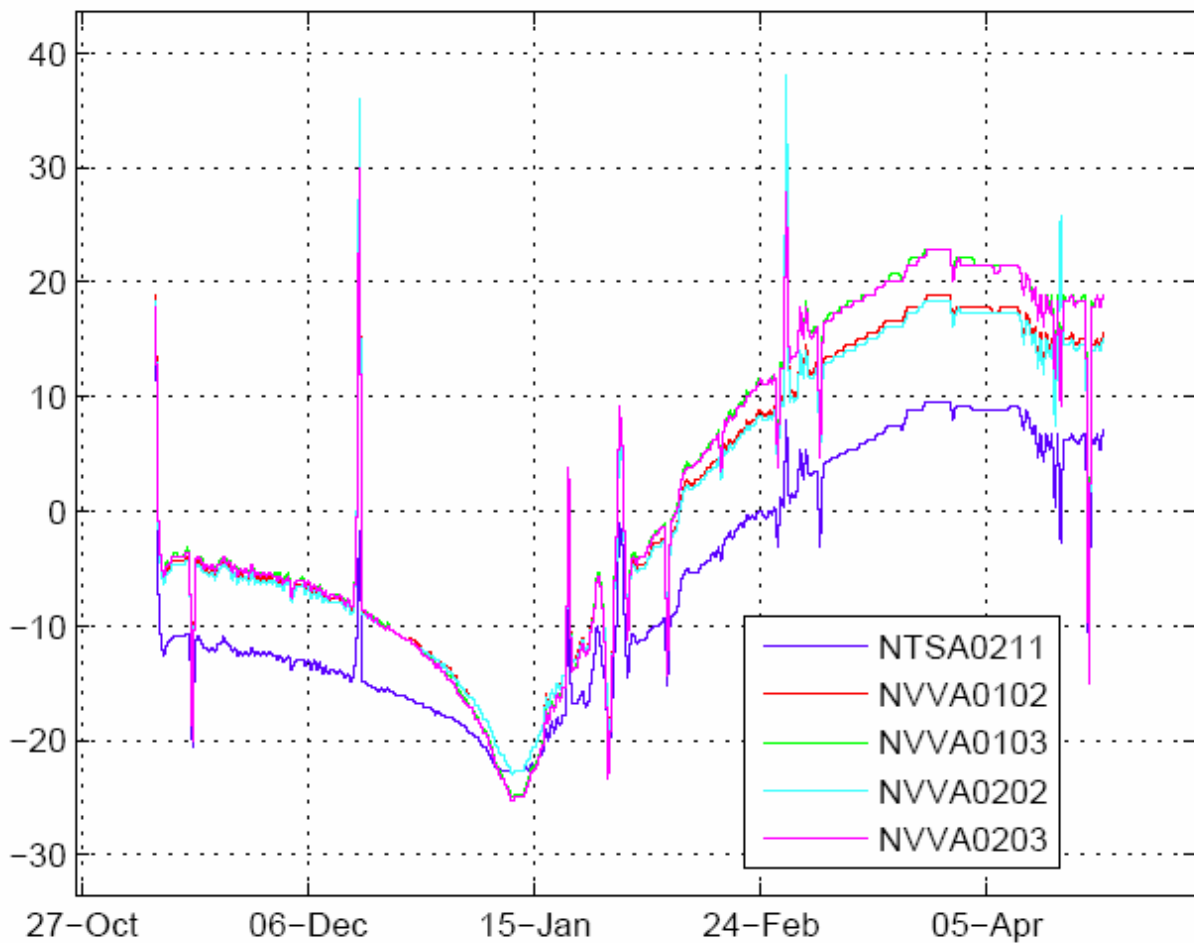


Figure 3.189 Temperatures measured during cruise and first orbital operations: CCD (green and magenta), DPU (red and cyan), THAVMC (VMC TRP ??) – blue.

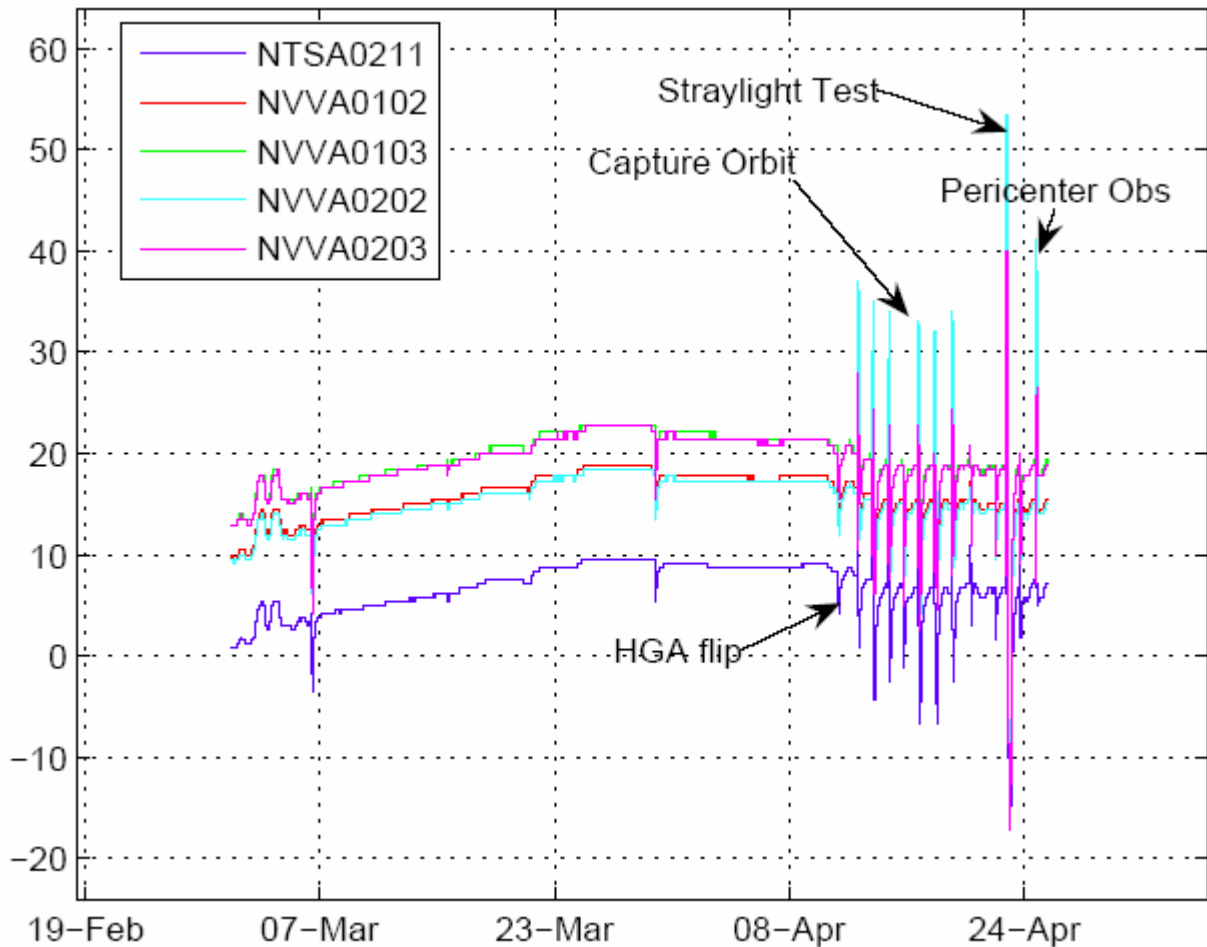


Figure 3.20 The same as in figure 3.18 for March-April, 2006.

4 Conclusions

- The VMC images taken after the orbit insertion show two types of signatures of degradation of the instrument performance: (1). dark stripe in UV image; (2).spots and filaments in all channels. Since none of the above mentioned features was present in the stray light images taken in February 2006 the degradation of the performance occurred in March –April during approach to Venus or VOI The processes that caused these damages are different.
- The dark stripe is caused by degradation (“yellowing”) of the microlenses under long exposure to the direct solar light during cruise.
- The origin of the spots and filament structures is still not understood. Original assumption that they are caused by thermal damage of the microlenses and CCD coating (that require

heating of the CCD to at least +150C) contradicts the temperature measurements on the CCD that did not exceed +40C.

5 Appendix A. Artifacts in VMC images (from R. Moissl's PhD thesis)

All throughout the mission two distinctive types of artifacts are present in the VMC raw images. Figure A.1 gives an example of the artifact patterns for all four channels in an early orbit. Most prominent and only occurring in the UV channel one can see a dark stripe across the middle of the image, ending in a circular feature. Present in all four channels, but with varying appearance is a pattern of bright polygonal filaments and bright and dark spots.

5.1 A.1 Dark UV strip

This feature is produced by discoloration (“yellowing”) of the polymeric micro lens layer due to UV radiation from the sun. During cruise phase The +Z-axis (and therefore the optical axis of VMC) has been pointed in the vicinity of the sun, producing an image of it onto the CCD. During the total duration of approximately 500 hours the position of the Sun on the CCD changed slowly along the path marked by the darkened stripe.

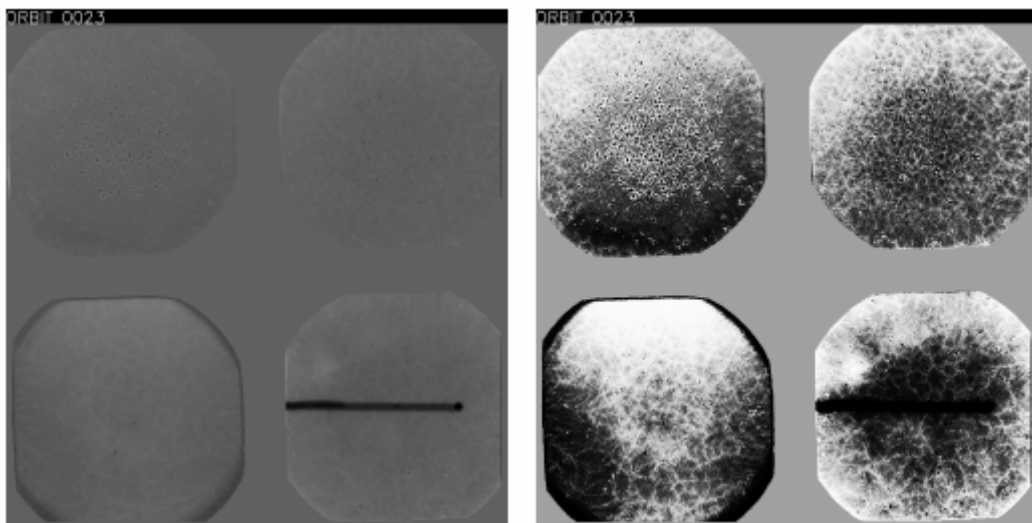


Figure A.1: Full CCD flat field patterns. Order of channels in both versions from top left in clockwise direction : Visible, IR1, UV, IR2. Left: Unenhanced flat field showing dark UV stripe. Right: Contrast-enhanced version showing filament and spot patterns in all four channels.

The sojourn time of the sun's image on each CCD pixel inside the dark strip correlates with the level of sensitivity degradation (see fig. A.2). The yellowing of the micro lens layer and resultant attenuation of UV signal is caused by chemical reactions in the polymer, triggered by sun UV radiation.

In the dark stripe signal levels are lowered by about 40% with respect to their surroundings. It has a mean width of ~17 pixels (corresponding to ~13mrad) and is orientated perpendicular to the CCD columns (in the XY plane of the spacecraft).

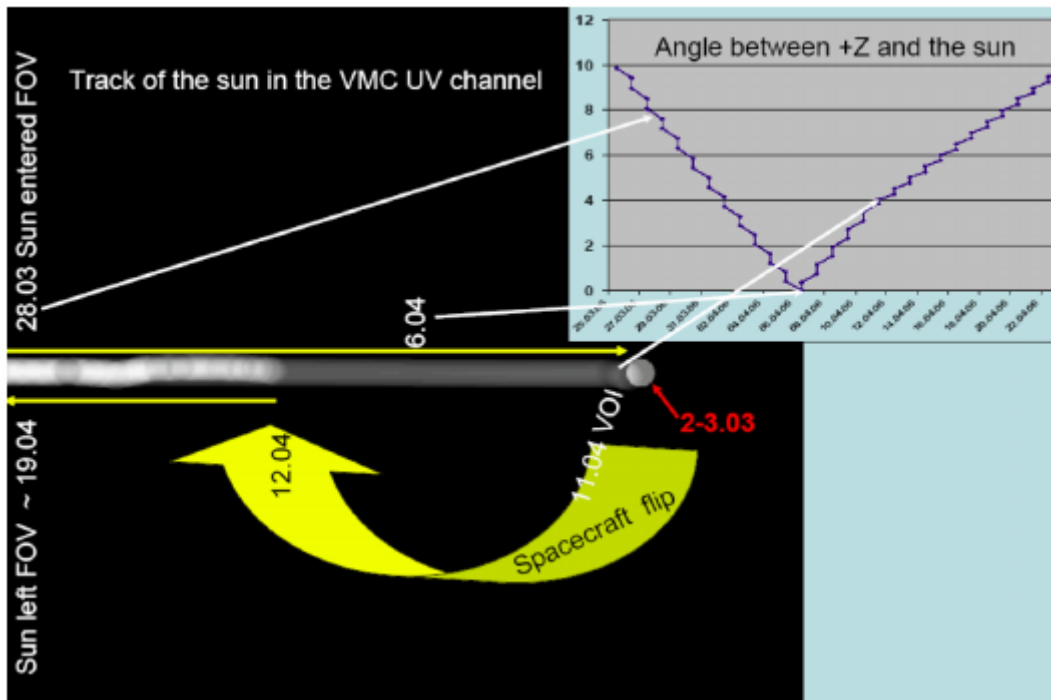


Figure A.2: Track of the Sun image on one quadrant of the CCD reconstructed from SPICE kernels. Brightness of the strip marks total illumination load.

The fact that direct UV radiation from the sun is darkening the micro lens layer led to the suspicion that UV radiation in general might lead to yellowing of the utilized polymer. In particular the relatively high flux of UV radiation reflected by the Venus upper cloud deck could possibly lead to progressive degradation of the UV channel. In order to investigate on a possible progressive degradation of the UV channel, I checked maximum, minimum and mean UV flux into the detector as a function of time throughout the first 670 Orbits. Figure A.3 shows mean flux (in $\text{DN} \cdot \text{s} \cdot 10^{-3}$) per image onto the CCD in the UV channel for dayside pericenter images versus orbit number. The periodic orbit-to-orbit variations are caused by brightness variations across the Venus disc due to the change of the orbital plane with respect to sun incidence angle. The higher fluxes in early orbits are to be attributed to non-linear response of the CCD in overexposed images. Ongoing adjustment of exposure times in later orbits prevented further overexposed images. The large variability of mean brightness per image inside most orbits is governed by the sun

aspect angle of the boresight intersection point on the cloud deck.

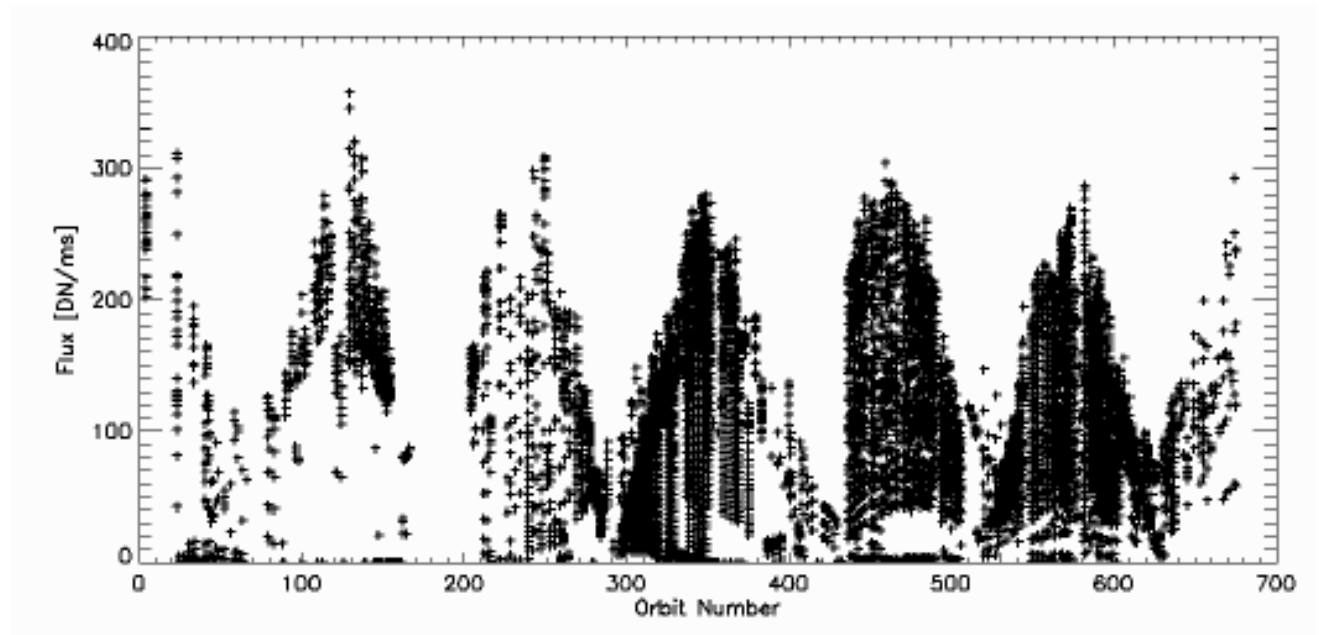


Figure A.3: Mean brightness per (pericenter) image as function of orbit number.

5.2 A.2 Filament-spot patterns

Contrary to the dark stripe, which apparently stays constant over time, the filament-spot pattern (further referred to as “FSP”) in all four channels keep evolving over time, displaying mainly erratic but partly cyclical behavior. Examples of appearance of the FSP during the mission are shown in figure A.4 .Detailed study of the FSP showed a number of properties summarized as follows:

1. The FSP includes bright filaments organized in polygonal (mainly hexagonal) shapes.
2. They also include dark spots of varying intensity and size. Smaller sized dark spots are characteristically darker than the larger ones.
3. Dark spots appear to be centered within the hexagonal filaments, giving a cell-like appearance to the FSP.
4. The FSP evolve over time. A widely observed behavior is shrinking size of dark spots and simultaneous darkening thereof.
5. Evolution of the FSP displays cyclic behavior. After dark spots have contracted completely, the cycle of shrinking starts again, usually with irregularly shifted “cells”.

6. Timescales of periodic changes seem to be not completely constant over time, but are on the order of 100-200 orbits.

7. Some bright filaments and more spread out dark spots seem to be slightly out of focus, but the small dark spots appear to be nearly always completely in focus.

8. Patterns are different in each channel, but general properties are common to all four channels. The IR1 and visible channels sometimes show symmetry about the image center, giving a rosette-like appearance.

This set of properties is strongly reminiscent of convective processes which tend to produce polygonal patterns. Keeping in mind that the observations are conducted in a space environment (vacuum, microgravity), the everyday observable Rayleigh-Bénard convection is very unlikely to be the cause of the FSP, since it is usually driven by density /buoyancy variations in liquids and gases (e.g. boiling water, heating in rooms). The Marangoni convection on the other side seems to be quite a promising candidate to explain the observed symptoms.

Marangoni instabilities arise from surface tension gradients on a gas-gas, liquid-liquid or gas-liquid interface in the presence of thermal gradients. Further no external gravity field nor constraints from aspect ratios between cell diameter and cell depth are required to trigger Marangoni convection.

One possible scenario is therefore that a thin polymeric layer close to the focal plane of the instrument either underwent a thermally induced phase change to a highly viscous film (not necessarily implying complete melting, for which temperatures have not been high enough at any time) or is reaching this state periodically during instrument operations. In both cases the CCD temperature, which varies roughly between 253K and 300K in the course of one orbit due to heat generated from the electronics, would provide a temperature gradient perpendicular to the CCD surface. Since evaporation processes can cause local inhomogeneities in surface tension, outgassing of compounds from a polymer film could provide the necessary random surface tension gradients to produce Marangoni instabilities. Some examples of patterns observed in laboratory experiments by Weh (2005) and Müller-Buschbaum (2003) are shown in figure A.5.

One important piece left in the puzzle is the question whether the polymeric micro lens layer can be identified to be the necessary highly viscous film where the Marangoni convection would be located. One indication against this hypothesis is the dark UV stripe, which is superimposed with the FSP and does not change in appearance at any time. If the micro lens layer would be the

location of the Marangoni convection at least some deformation of the borders of the UV stripe should be expected. Since this is not the case, we studied the technical specification Manual for the Kodak KAI-1010M CCD chip used in the VMC. Figure A.6 shows a series of detailed sketches of the chip. In addition to the micro lens layer, an epoxy layer with a thickness of 0.05mm-0.18mm is located 2mm away from the CCD surface. This epoxy layer would be another possible location for the FSP.

In conclusion we propose with some confidence, that the FSP in VMC images are being caused by Marangoni convection either in parts of the micro lens layer or in the epoxy film on the cover glass on top of the CCD. Unfortunately the limited time available precluded further analysis of this interesting topic.

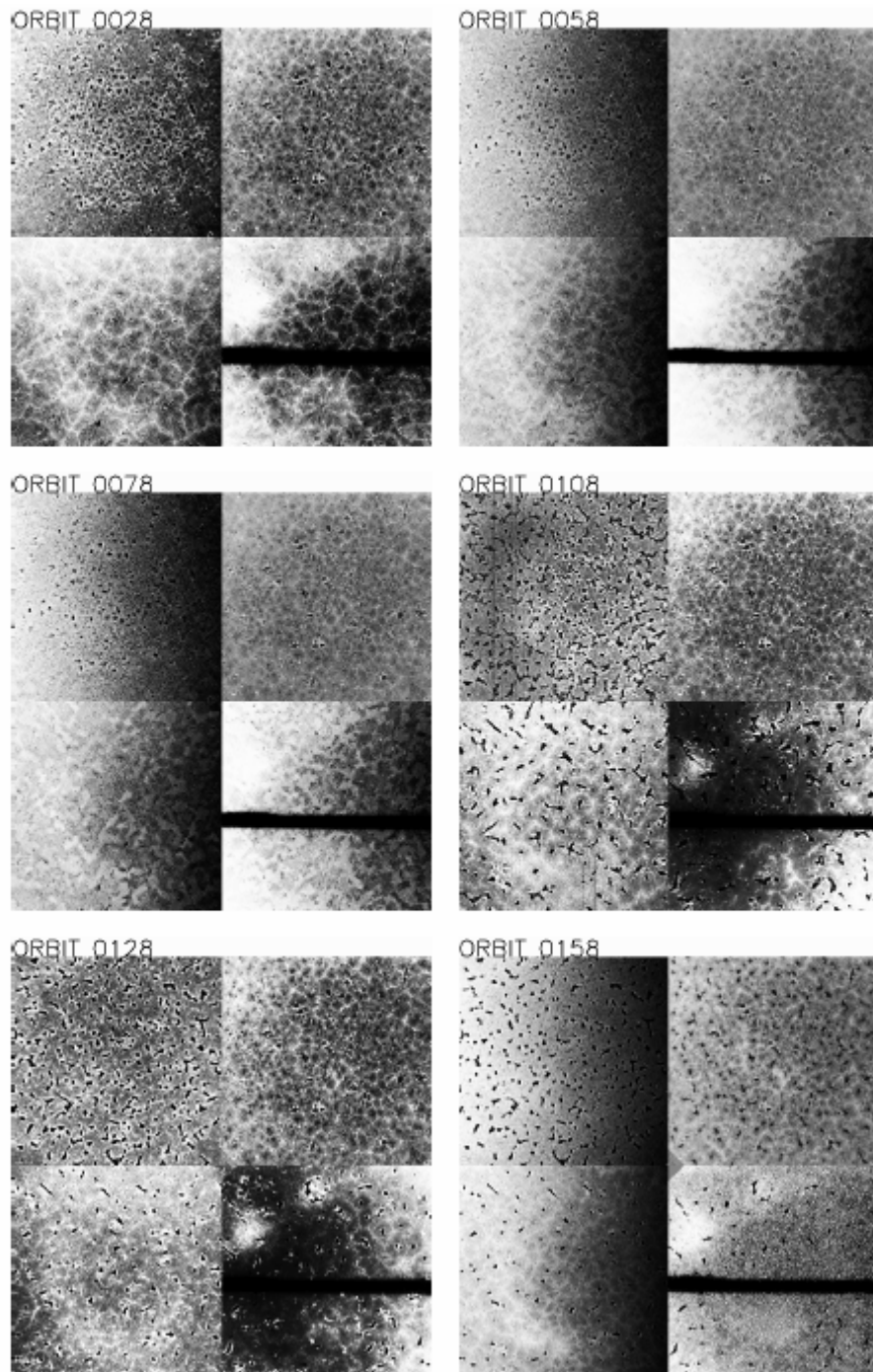


Figure A.4: Excerpts of flat fields from all four channels in di_ erent orbits.

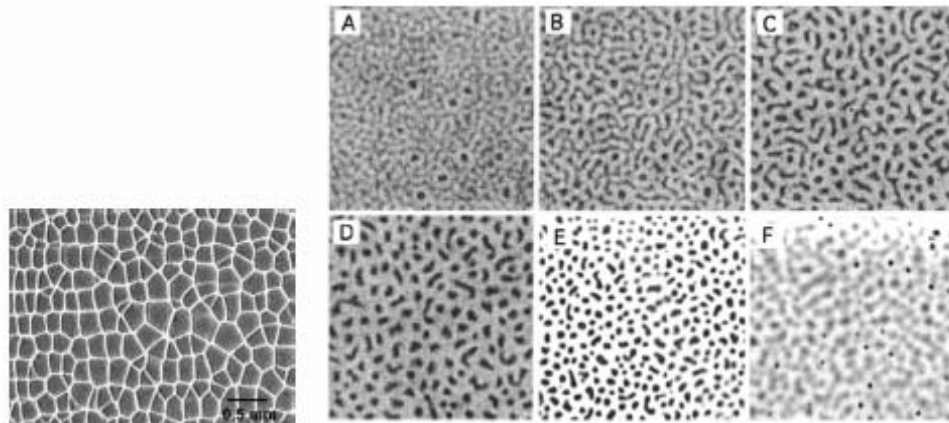


Figure A.5: Examples of patterns resulting from Marangoni convection in thin polymer layers. Left: Marangoni convection pattern from Weh (2005). Right: Time series of developing Marangoni convection from Müller-Buschbaum (2003).

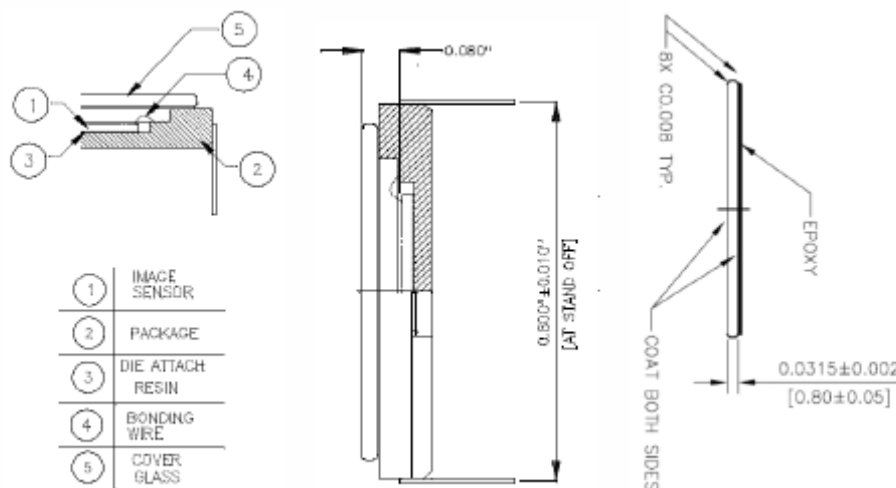


Figure A.6: Detail sketches of Kodak KAI-1010M. Left: Description of chip structure. Middle: Dimensions. Right: Detail sketch of the cover glass, mentioning a thin epoxy layer.